W&M ScholarWorks

Dissertations, Theses, and Masters Projects   Theses, Dissertations, & Master Projects

1965

Bremsstrahlung Production in Lanthanum Thick Targets

David Neil Ferguson
College of William & Mary - Arts & Sciences

Follow this and additional works at: https://scholarworks.wm.edu/etd

Part of the Physics Commons

Recommended Citation

BREMSSTRAHLUNG PRODUCTION IN LANTHANUM THICK TARGETS

A Thesis

Presented to

The Faculty of the Department of Physics

The College of William and Mary in Virginia

In Partial Fulfillment

Of the Requirements for the Degree of

Master of Arts

By

David Neil Ferguson

November 1965

ProQuest Number: 10624990

ProQuest.

ProQuest 10624990

APPROVAL SHEET

This thesis is submitted in partial fulfillment of

the requirements for the degree of

Master of Arts

David Neil Ferguson
Author

Approved, November 1965:

Morton Eckhause
Morton Eckhause, Ph.D.

Robert E. Welsh
Robert E. Welsh, Ph.D.

Herbert Funsten
Herbert Funsten, Ph.D.

ii

ACKNOWLEDGMENTS

TABLE OF CONTENTS

LIST OF FIGURES

ABSTRACT

Bremsstrahlung radiation with an energy greater than 0.4 MeV produced by 1.0 MeV electrons incident on thick lanthanum (Z = 57) targets has been investigated. Laboratory provisions were made for the measurement of the spatial and energy distribution of the radiation. Experimental data are graphically presented in terms of the bremsstrahlung intensity, $I(\theta_0)$, and the differential cross sections $\dfrac{d\sigma}{dk\,d\theta_0}$, and $\dfrac{d\sigma}{dk}$. Also, the efficiency for production of high energy photons is given. The experimental data are presented in conjunction with theoretical values.

BREMSSTRAHLUNG PRODUCTION IN LANTHANUM THICK TARGETS

INTRODUCTION

In passing through matter electrons lose kinetic energy by excitation and ionization of atomic electrons and by radiative emission in the field of the nucleus and the electrons. In the excitation and ionization interactions, electromagnetic energy is given off in the form of characteristic X-rays. The characteristic X-rays have discrete energies over a limited range, the extent of which depends on the electron energy-level structure of the atom. For lanthanum, the highest energy characteristic X-ray is about 38 keV. In this work we measured X-rays in the range 400 keV to 1000 keV and ignored the characteristic X-ray spectrum. Electron-electron bremsstrahlung, which is expected to be less than 2 percent (ref. 1) of electron-nucleus bremsstrahlung in lanthanum, was also ignored.

When encountering large electric field gradients arising from the nuclear charges, electrons may easily be deflected. Upon deflection, the electron may lose some of its energy by emitting electromagnetic radiation known as bremsstrahlung. In the emission process an incident electron of momentum $\bar{p}_0$ and energy E_0 is deflected by the nuclear field and emits radiation with momentum $\hbar\bar{k}$. The electron is then left with momentum $\bar{p}$ and energy E.

The probability of radiative emission by an electron depends strongly on the distance of the electron from the nucleus. Bremsstrahlung emission occurs when an electron is at a distance of the order of $\frac{\hbar}{q}$ (ref. 1) from the nucleus where q is the recoil momentum given to the atom in the radiation process as permitted by conservation of energy and momentum. If the effective impact parameter, $\frac{\hbar}{q}$, is large compared with the nuclear radius and small compared with the atomic radius, we may ignore the charge distribution of the nucleus and the screening of the nucleus by the atomic electrons. We may then consider the field acting on the particle during the radiation process as the Coulomb field of a point charge, Ze, at the center of the nucleus. If the effective impact parameter is large compared with the atomic radius, the screening effect of the atomic electrons will play an important role. Finally, if the impact parameter is small compared with the nuclear radius, then we may not consider the electric field acting on the particle as that arising from a point charge.

The bremsstrahlung process does indeed occur at distances from the nucleus large compared with the nuclear radius (ref. 2). Thus, it is correct to consider the nucleus as a point charge. The relevant parameter for assessing the importance of electron screening is defined as

$$\xi = \frac{100 \ mc^2 h\nu}{E_o E Z^{1/3}}$$

where

E_O = initial electron energy, MeV

E = final electron energy, MeV

$h\nu$ = E_O - E, MeV

mc^2 = rest mass energy of electron, MeV

Z = atomic number of target nuclei

This measure of screening has been calculated by Bethe and Heitler on the basis of the Fermi-Thomas model of the atom (ref. 3). When $\xi \gg 1$, the screening may be neglected, whereas for $\xi = 0$, the screening is practically complete. For the experimental effort reported herein, the smallest photon energy considered is $h\nu \approx 0.400$ MeV and the incident energy is E = 1.0 MeV. For these values $\xi \approx 9$. Thus, screening is neglected in this analysis.

It is very difficult to properly predict the trajectory of the electron after radiative emission. If we neglect the loss of energy through radiative emission, then the electron should follow a hyperbolic trajectory in its orbit about a positive nucleus. The theoretical spectral distribution of the radiation emitted by electrons in hyperbolic orbits about nuclei was calculated by Kramers. However, the experimental data did not bear out his theoretical calculations (ref. 4). In 1919, Webster (ref. 5) suggested that electrons traversing matter were set into oscillatory motion. Thus, the electrons would be moving radiators as they pass through the target material. This oscillating electron model could not be confirmed by experimental evidence (ref. 5). Nicholas (ref. 6) in 1929 attempted to account for the bremsstrahlung spectrum by proposing that the electric charge density

of a uniform moving electron had a wave form similar to an electromagnetic wave. This proposal was inconsistent with experiments on electron diffraction and was abandoned. Classical attempts to account for the continuous bremsstrahlung spectrum always met failure.

Contrastingly, the initial applications of quantum principles to the problem of a continuous bremsstrahlung spectrum were more successful than the classical theories. According to quantum electrodynamics, there is a finite probability that an electron traversing in the field of a nucleus will make a radiative transition to another state with the emission of a photon. Interaction with the field of a nucleus is necessary to conserve energy and momentum since it is impossible for a free electron to emit a single photon and make a transition to a real state. The nucleus, because of its large mass, does not acquire any large portion of the energy, but may acquire a transverse momentum comparable with the transverse momentum of the electron and photon. Therefore, the conservation laws of momentum and energy permit an electron to emit photons of the same energy in different directions and a relation between energy and angle of emission of the photon in a radiation process is not furnished by these conservation laws. The quantum mechanical treatment of the bremsstrahlung phenomenon by Bethe and Heitler (ref. 3) has formed the basis from which various authors have derived bremsstrahlung cross-section formulas at different levels of sophistication. The results of these calculations have been presented in a summary article by Koch and Motz (ref. 7).

In the formalism used by Koch and Motz, the cross section for bremsstrahlung emission in a cube with sides L is given by the transition

probability per atom per electron divided by the incoming electron velocity. The cross section is expressed as

$$d\sigma = \frac{w}{(p_oc/E_o)}\left(\frac{h}{m_oc}\right)^3 L^3$$

where

$$w = \frac{2\pi}{h}\,\rho_f\left|H_{if}\right|^2$$

$$\rho_f = \text{density of final states} = \frac{pEk^2 dk d\Omega_k d\Omega_p L^6}{(2\pi)^6 m_o c^2}$$

H_{if} is the transition matrix and $\left|H_{if}\right|^2$ is written as

$$\left|H_{if}\right|^2 = \left(\frac{2\pi e^2}{khc}\right)(m_oc^2)^2\left|\int \psi_f^* (\bar{\lambda}^* \cdot \bar{\alpha})e^{-i\bar{k}\cdot\bar{r}}\,\psi_i dr\right|^2 L^{-9}$$

$\bar{\lambda}$ is the unit polarization vector of the photon, $\bar{\alpha}$ is the Dirac matrix and ψ_i and ψ_f are the initial and final Dirac wave functions for the electrons. In considering the electron-nuclear interaction, $V = \frac{Ze^2}{r}$, the Born approximation, which assumes $\frac{2\pi Z}{137\beta} \ll 1$, has been used to obtain the explicit differential bremsstrahlung cross sections. With the assumption that the nuclear Coulomb field is unscreened by the atomic electrons, the corss-section differential in photon energy and emission angle as developed in the summary article, Formula 2BN, may be written as below with some rearrangement of terms:

$$\frac{d\sigma}{dkd\theta_0} = \frac{Z^2}{137(4)} \frac{r_0^2}{k} \frac{p}{p_0} \sin\theta_0 \left\{ \frac{8 \sin^2\theta_0(2E_0^2 + 1)}{p_0^2\Delta_0^4} - \frac{2(5E_0^2 + 2EE_0 + 3)}{p_0^2\Delta_0^2} \right.$$

$$- \frac{2(p_0^2 - k^2)}{Q^2\Delta_0^2} + \frac{4E}{p_0^2\Delta_0} + \frac{L}{pp_0}\left[\frac{4E_0 \sin^2\theta_0(3k - p_0^2E)}{p_0^2\Delta_0^4} + \frac{4E_0^2(E_0^2 + E^2)}{p_0^2\Delta_0^2} \right.$$

$$\left. + \frac{2 - 2(7E_0^2 - 3EE_0 + E^2)}{p_0^2\Delta_0^2} + \frac{2k(E_0^2 + EE_0 - 1)}{p_0^2\Delta_0} \right] - \left(\frac{4\epsilon}{p\,\Delta_0} \right)$$

$$\left. + \left(\frac{\epsilon^Q}{p^Q} \right)\left[\frac{4}{\Delta_0^2} - \frac{6k}{\Delta_0} - \frac{2k(p_0^2 - k^2)}{Q^2\Delta_0} \right] \right\}$$

where

$$L = \ln\left(\frac{EE_0 - 1 + pp_0}{EE_0 - 1 - pp_0} \right)$$

$$\Delta_0 = E - p_0 \cos\theta_0$$

$$\epsilon = \ln\left(\frac{E + p}{E - p} \right)$$

$$\epsilon^Q = \ln\left(\frac{Q + p}{Q - p} \right)$$

$$Q^2 = p_0^2 + k^2 - 2p_0 k \cos\theta_0$$

This gives the probability that for an incident electron of energy E_0, a quantum of momentum $\bar{k}$ is emitted at an angle θ_0 to the direction of the incident electron, and that the scattered electron of momentum $\bar{p}$ proceeds in a direction given by polar angles β, ϕ, referred to $\bar{k}$.

Figure 1 shows the geometry for bremsstrahlung emission. The incoming and outgoing electron states each has two possible spin states and the outgoing photon can be polarized in any direction. However, we are not interested in the direction of the spin or the polarization of the photon. Hence a summation over the photon and outgoing electron polarizations and an averaging over the initial polarizations of the electron have been performed in deriving the cross-section formula.

Employing the same considerations as used in deriving the formula for $\dfrac{d\sigma}{dk d\theta_0}$, Koch and Motz presented an expression, Formula 3BN, for the bremsstrahlung cross-section differential in photon energy. It is essentially the following:

$$\frac{d\sigma}{dk} = \frac{Z^2 r_0{}^2 p}{137 k p_0}\left\{\frac{4}{3} - 2E_0E\left(\frac{p^2 + p_0{}^2}{p^2 p_0{}^2}\right) + \frac{\epsilon_0 E}{p_0{}^3} + \frac{\epsilon E_0}{p^3} - \frac{\epsilon\epsilon_0}{p_0 p} + L\left[\frac{8E_0 E}{3p_0 p}\right.\right.$$

$$\left.\left. + \frac{k^2(E_0{}^2 E^2 + p_0{}^2 p^2)}{p_0{}^3 p^3} + \frac{k}{2p_0 p}\left(\left(\frac{E_0 E + p_0{}^2}{p_0{}^3}\right)\epsilon_0 - \left(\frac{E_0 E + p^2}{p^3}\right)\epsilon + \frac{2kE_0 E}{p^2 p_0{}^2}\right)\right]\right\}$$

where

$$L = 2\ln\left(\frac{E_0 E + p_0 p - 1}{k}\right)$$

$$\epsilon_0 = \ln\left(\frac{E_0 + p_0}{E_0 - p_0}\right)$$

$$\epsilon = \ln\left(\frac{E + p}{E - p}\right)$$

These cross-section formulas have been used in a computer program for theoretical calculations.

The angular distribution, $I(\theta_o)$, of the emitted radiation is almost prohibitively complicated when the electron energy is comparable with the rest mass energy of the electron (ref. 1) and no general analytical or empirical formula correctly expressing the distribution is available. In previous bremsstrahlung measurements (ref. 7) it has nevertheless been noted that even in cases where use of the Born approximation seemed unjustified theoretical estimates based on it have shown reasonable agreement with measured values. The bremsstrahlung energy intensity emitted in a certain direction θ_o is obtained by multiplying the number of photons of energy k, $\dfrac{dn(k)}{d\theta_o}$, by the photon energy and integrating over all photon energies

$$I(\theta) = \int_{0.4\text{ MeV}}^{1.0\text{ MeV}} k\, \frac{dn(k)}{d\theta_o} dk$$

The total radiated energy between 0.4 and 1.0 MeV is then simply calculated by integrating $I(\theta_o)$ over all directions in space.

CHAPTER I

EXPERIMENTAL APPARATUS AND PROCEDURE

General

The experimental assembly is shown in figure 2 and figure 3. A cylindrical brass target chamber was mounted at the end of the accelerator beam tube. Thick targets were positioned at the center of the chamber. The electron beam was focused on the target and struck it at normal incidence. In order to measure the total number of electrons incident on the target and the number backscattered onto the chamber, it was necessary to electrically isolate the chamber from both the beam tube and the supporting distribution table. By use of vacuum pumping systems, the pressure in the target chamber was reduced to approximately 1×10^{-5} millimeters of mercury during the measurements. For convenience and for protection of equipment, vacuum valves were placed in the beam tube assembly. One valve of particular importance was the gate valve between the target chamber and the beam tube. Use of this valve permitted opening the target chamber without opening the beam tube to atmospheric pressure.

Targets

Targets used in the experiment were thick targets, that is, thick enough that incident electrons expended all their kinetic energy in traversing the target. The thickness of the target was determined from

the following Katz and Penfold (ref. 8) relation for the range of
electrons:

$$R(mg/cm^2) = 412E^n$$

where

n = 1.265 - 0.0954 $\ln$ E

E = kinetic energy of the electron in MeV

To assure negligible transmission, the actual target thickness was made
10 percent greater than the range R. High purity lanthanum targets
(Z = 57), 0.0288 inch thick, were prepared for use with 1.0 MeV electrons.
The targets were circular with 1.0 inch diameter. To maintain cleanli-
ness and to suppress oxidation, the targets were stored in an inert
nitrogen atmosphere when not in use.

Target Chamber

The target chamber was a brass cylinder 8 inches in diameter and
5 inches deep. As shown in figure 4, the chamber was mounted at the
center of a 32-inch-diameter steel table, the perimeter of which was
marked such that the angular position of the detector assembly could be
accurately known to ± 0.25°. For viewing purposes, a 1/2-inch-thick
quartz cover was fitted to the top of the chamber. The chamber wall was
made very thin (approximately 0.03 inch) at selectively spaced positions
along one side of the chamber to minimize attenuation of the penetrating
bremsstrahlung and thereby increase the statistical accuracy of the
spectral measurements at the five angular settings of 15°, 45°, 75°,
105°, and 135°. The zero degree reference position was taken as the
centerline of the beam tube. A small shaft through the chamber wall was

connected to a remotely controlled motor which would rotate a zinc-
sulfide backed piece of titanium into the target position. Alignment
of the electron beam was achieved through television observation of the
fluorescent pattern created by electrons normally incident on the zinc-
sulfide surface.

Electron Beam Current Integration

It was necessary to know the number of electrons incident on the
target for a given run. This was accomplished by electrically connect-
ing the target to an Elcor current integrator which registered a
cumulative count of the electrons striking the target. All electrons
entering the chamber were directed at the target, but an appreciable
fraction of these were backscattered from the target onto the chamber
walls. The number of electrons so striking the chamber was measured
in the same way as for the target. During all runs, the current incident
on the target was kept at about 2×10^{-9} amperes.

Detecting System

Bremsstrahlung leaving the target at an angle θ_o to the incident
beam passed through a 1/2-inch-diameter by a 6-inch-long collimating
channel in a lead cylinder which enclosed a scintillation detector. The
lead shielded the detector so that only those photons reaching the
detector through the collimating channel would be counted. The detector
was a 2-inch by 2-inch sodium iodide, thallium activated crystal mounted
on a Dumont 6292 photomultiplier tube. As shown in figure 5, the detector
was 3 feet from the target so that the spot at which electrons struck
the target could be approximated by a point source of bremsstrahlung to

the detector. The detector assembly was on a movable support which permitted horizontal angular variation of the detector position while keeping its radial distance from the target constant. Another detector of the same type was placed on the distribution table on the other side at an angle of 60° to the beam direction. This latter detector acted as a monitor in providing an instantaneous indication of the bremsstrahlung intensity at all times. By noting variations in count rate as registered by this detector, we were made aware of fluctuations in the electron beam intensity and energy at the target position. The electronic circuitry consisted essentially of an emplification system which fed pulses into a TMC 400-channel pulse height analyzer and storage unit (Model No. 402). Spectral data in the analyzer's memory were electronically printed out with an IBM typewriter.

Correction for Background

Bremsstrahlung spectra obtained for the lanthanum target necessarily included a background contribution. This background contribution can be assumed to arise only from the bremsstrahlung created by backscattered electrons striking the brass target chamber, since the detectors were so shielded that any radiation inadvertently produced anywhere except in the target chamber could not be counted. From the diagram below, it is seen that when the target is in position, Q_2 is the total charge backscattered onto the target chamber.
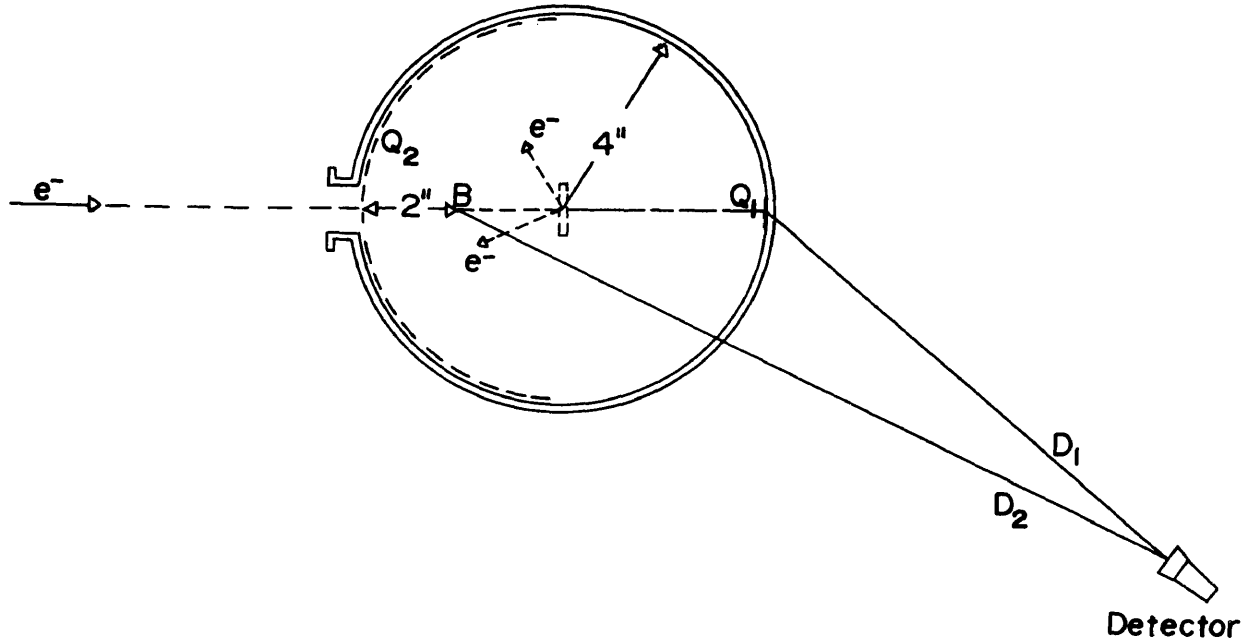
Backscattering should be symmetrical about the incident beam so we have taken the point B as the effective site of background sources. With the target removed, we let a charge Q_1 strike the wall of the chamber and register C_1 counts. Then, since the number of photons detected at a given position is proportional to the total incident electron flux creating the bremsstrahlung and is inversely proportional to the square of the distance from source to detector, the counts arising from charge Q_2 would be given as

$$C_2 = C_1 \left(\frac{D_1{}^2}{D_2{}^2}\right)\left(\frac{Q_2}{Q_1}\right)$$

This then is the background subtraction (after correction for counting rate effects) from spectral measurements obtained with targets in position and an accumulated backscattered charge Q_2. By interpolation of experimental data (ref. 9), it is found that when 1.0 MeV electrons impinge normally on lanthanum, the backscattered electrons have an average energy of about 0.7 MeV. In assessing the background contribution, we have not accounted for this energy difference because the total background contribution is very small. Hence, any error entailed in ignoring the energy difference would be negligibly small.

CHAPTER II

COMPUTATIONAL MODEL

The cross-section formula as presented pertains to the case in which a single electron normally incident on the target collides with an atom and is deflected from its original direction and emits a photon. This is an idealized situation, for in the thick-target case the electron may experience many deflective collisions before bremsstrahlung emission or termination of its traversal of the target. To obtain theoretical estimates of the bremsstrahlung spectrum, we must therefore establish a physical model which appropriately represents the thick-target case. Such a physical model has been established and programed* for computer use in predicting bremsstrahlung spectra, and theoretical values obtained with it are presented along with experimental results. The thick target is divided into a large number of equal energy loss strips, thereby approximating a laminar structure of thin targets. Each strip is of such thickness that an incoming electron loses 10 KeV of its kinetic energy as it circuitously traverses the strip. It is assumed that all incident electrons are stopped in the target with none backscattered. The angular distribution of electrons resulting from multiple scattering in each strip is calculated using the

_____

*Theoretical values have been provided by Chris Gross, NASA, Langley Research Center, Hampton, Virginia.

Goudsmit-Saunderson theory (ref. 10). The progress of the electron is followed by simply letting it pass incrementally through a series of energy values ranging from E_0 to 0.

For the purpose of determining the electron distribution, it was assumed that the electron loses energy only by collision with atomic electrons. This is a valid approximation for electrons of a few MeV or less, for at these energies the neglected bremsstrahlung energy loss is only a small fraction of the total energy loss (ref. 1). The distribution in energy and direction of the electron is determined for every 10 keV interval between E_0 and 0. As used in these computations, the Goudsmit-Saunderson angular distribution formula for multiple scattering deflections is given by (ref. 11)

$$A_{GS}(\eta) = \sum_{l=0}^{L} \left(l + \frac{1}{2} \right) \exp \left[- \int_{0}^{s} G_l(s')ds' \right] P_l(\cos \eta)$$

where

$$G_l(s) = 2\pi N \int_{0}^{\pi} \sigma(\mu,s) \left[1 - P_l(\cos \mu) \right] \sin \mu \, d\mu$$

and individual parameters are defined as follows:

$A_{GS}(\eta)$ = scattered electron intensity in the direction η

η = the direction of the electron after experiencing multiple scattering in traversing s

μ = the direction of the electron after its first collision

$\sigma(\mu,s)$ = cross section for electron single scattering through an angle μ

s = pathlength traversed between each 10 keV energy interval

L = value of the Legendre polynomial index at which convergence is achieved

N = atomic density of the target material

The geometry for bremsstrahlung production is depicted in figure 1.

Having determined the number of electrons of a given energy and direction, one uses the Bethe-Heitler bremsstrahlung cross section to estimate the bremsstrahlung distribution according to the formula

$$I(\theta_o,k) = \int_o^E \int_o^\pi \int_o^{2\pi} N(E)A_{GS}(\eta)\left(\frac{d\sigma}{dkd\theta_o}\right)e^{-\frac{\mu(k)t}{2\cos\theta_o}}\, d\phi\, d\eta\, dE$$

where $N(E)$ is the number of atoms which may be encountered by an electron of energy E; $\mu(k)$ is the coefficient for target absorption of bremsstrahlung photons of energy k; and t is the target thickness. In computing the photon absorption it was assumed that all photons emanated from the physical midpoint of the target. The triple integral is then the bremsstrahlung intensity of energy k at emission angle θ_o.

CHAPTER III

DATA ANALYSIS

The measured bremsstrahlung spectra at 45° and 105° are presented
in figure 6 and figure 7. These are representative of the spectra at
all angles. These figures present the raw data which have not been
corrected for background, counting rate, and absorption effects. The
corresponding raw background spectra are presented in figure 8 and
figure 9.

After background and counting rate corrections, the next step in
data analysis was that of "stripping" the spectrum. Stripping is
necessary because the scintillation detector is incapable of making
faultless energy identification of the photons. That is, upon detection,
photons of a discrete energy can register as having an energy spread
ranging from zero to the full photon energy. Hence, resolution
inaccuracies are inherent in the spectral data. To correct for this
resolution error, one must obtain a representation of the crystal's
resolution characteristics. This is accomplished by recording the calibra-
tion spectra obtained from monoenergetic gammas emitted by Na^{22} (0.51 and
1.28 MeV), Cs^{137} (0.667 MeV), and Co^{60} (1.17 and 1.33 MeV). These calibra-
tion spectra are shown in figures 10 and 11. The contribution in counts
from the Co^{60} 1.33 MeV peak to the 1.17 MeV peak was obtained by first
noting that the energy difference between these two peaks is 0.16 MeV.
Then, referring to the 1.28 MeV peak of Na^{22}, the number of counts in

the channel corresponding to 1.28 - 0.16 = 1.12 MeV was taken as the
contribution which the Co^{60} 1.33 MeV peak made to the 1.17 MeV peak.
By this procedure the correct number of counts p in the 1.17 MeV peak
was ascertained. In the spectrum from Na^{22} as shown in figure 10, the
count level due to the 1.28 MeV gammas was approximately constant between
channels 120 and 220. Then, by extrapolating this constant count level
to the left, we determined the contribution under the 0.511 MeV peak due
to the 1.28 MeV gammas. Thus, we estimated the number of counts in the
0.511 MeV peak.

By determining the area under each of these calibration curves, we
obtain the total number of counts attributable to each of these discrete
energy photons. Then, knowing the height p (in counts) of the total
capture peak in each of these calibration spectra, the ratio of peak
height to total counts is determined. These ratios are characteristic
of the detector used in the present investigation and are plotted as a
function of photon energy.

Upon dividing the bremsstrahlung spectrum into 50 keV wide brackets,
a profile of the nearest energy calibration peak is superimposed on the
highest energy bracket. The calibration profile is then matched to the
mean height of the 50 keV energy bracket. This profile of an accurately
known monoenergetic photon established a pulse representation for that
particular mean energy in the increment. By subtraction of the profile
from the spectrum, the contribution of that pulse was removed. The same
procedure was followed for all the remaining 50 keV wide brackets. For
each bracket, the mean photon energy and the corrected total capture peak
intensity are then known. By referring to the calibration curve of peak

intensity to total counts plotted against energy, one can determine the
ratio for the mean bracket energy. With this ratio and the total capture
peak intensity, one can determine the corrected number of photons at each
mean energy. Additionally, the detection efficiency of the sodium iodide
crystal was a function of photon energy as shown in figure 12 (ref. 12).
Hence, a correction for detector efficiency was applied along with a final
correction for bremsstrahlung attenuation in the aluminum cover of the
crystal and the walls of the target chamber. No correction was made for
photon absorption in the target, as a numerical evaluation of the exponential
attenuation function indicated that absorption of photons in the energy
range we are considering was negligibly small. Stripping and application
of the corrections transformed the data to a form which could be compared
with theory.

CHAPTER IV

EXPERIMENTAL RESULTS

Angular Distribution

The measured angular distribution of 0.4 MeV to 1.0 MeV photons

is shown in figure 13. For comparison, the angular distribution as

predicted by the theoretical model is also presented.

For incident electrons of an energy comparable with the electron

rest energy, no general analytical or empirical formula correctly

expressing the angular distribution of thick-target bremsstrahlung is

available. Using a least squares curve fitting procedure with the

five measured values on the experimental curve, an expression for the

angular distribution having a maximum of four terms was permitted.

The formula was expressed in terms of arbitrarily chosen Legendre

polynomial functions having the form

$$W(\theta_o) = \alpha_o + \alpha_1 P_1(\cos \theta_o) + \alpha_2 P_2(\cos \theta_o) + \alpha_3 P_3(\cos \theta_o)$$

where the coefficients were found to have the following values:

$$\alpha_o = 8.42 \times 10^{-6} \qquad\qquad \alpha_2 = 3.45 \times 10^{-6}$$

$$\alpha_1 = 6.56 \times 10^{-6} \qquad\qquad \alpha_3 = 2.10 \times 10^{-6}$$

Cross-Section Differential in Photon Energy and Angle

The differential cross section, $\dfrac{d\sigma}{dk d\theta_o}$, for production of photons

of energy in the range k and $k + dk$ at an angle between θ_o and

22

θ_0 + $d\theta_0$ is presented in figures 14 through 18 as a function of photon energy. It is emphasized that these values constitute a thick-target measurement of the cross section in contrast to the values one might obtain in the more idealistic case of a thin-target measurement. This point is stressed because of the difference between the thick-target case in which the electron is multiply scattered in its traversal of the target and the thin-target case in which the electron is singly scattered through a negligibly small angle in passing through the target.

Integrating $\frac{d\sigma}{dkd\theta_0}$ over angles yields $\frac{d\sigma}{dk}$, the differential cross section for production of photons of energy in the range k and k + dk. Measured and theoretical values are shown in figure 19.

Efficiency for Bremsstrahlung Production

When electrons expend all of their kinetic energy in the target, the efficiency for bremsstrahlung production is the ratio of bremsstrahlung radiated to the energy of the incoming electron. The total energy, I, radiated as photons having energies from 0.4 MeV to 1.0 MeV is obtained by integrating the intensity $W(\theta_0)$ over all angles:

$$I = \int W(\theta_0)d\Omega = 2\pi \int_0^{\pi} W(\theta_0)\sin \theta_0 \, d\theta_0$$

From this integration, it was found that the experimental value for the efficiency for bremsstrahlung in the range 0.4 MeV to 1.0 MeV is 0.63 percent. The computational model predicted an efficiency of 0.51 percent.

CHAPTER V

CONCLUSIONS

From the data presented herein, the following conclusions are
derived:

1. (a) Using the computational model described herein, computed
values of the bremsstrahlung intensity for photons of energy greater than
0.4 MeV are below the measured values at all angles as shown by comparison
in figure 13. It is also shown that the difference between these theoreti-
cal and experimental values decreases with increasing emission angle.

2. (a) As shown in figure 14 through figure 18, the experimental
differential cross section, $\frac{d\sigma}{dkd\theta_o}$, is a smoothly decreasing function of
photon energy at all angles.

(b) Measured values of the differential cross section at
photon energies greater than about 0.7 MeV are below the calculated
estimates; for smaller energies the reverse is true. This difference is
attributed in part to the fact that experimental measurements with thick
targets are complicated by electron backscattering from the target.
However, the theoretical and experimental results are in agreement
within a factor of 2 at all photon energies.

(c) At smaller photon energies, experimental values of $\frac{d\sigma}{dkd\theta_o}$
are of the same order of magnitude for all angles, whereas at the higher

photon energies their magnitude varies greatly with angle. For example, at a photon energy of 0.40 MeV, $\frac{d\sigma}{dkd\theta_0}$ for the 15° case is 3.3 times $\frac{d\sigma}{dkd\theta_0}$ at 135°, but at 0.97 MeV the value at 15° is 60 times that at 135°.

(d) In general, experimental and theoretical values of $\frac{d\sigma}{dkd\theta_0}$ tend toward closer agreement at backward angles.

3. (a) The reasonably good agreement between the experimental efficiency (0.63 percent) and the computed value (0.51 percent) affirms the general adequacy of the computational model in which the Born approximation has been employed under conditions where it is expected to fail.

REFERENCES

1. Segre, E.:   Experimental Nuclear Physics.   1, John Wiley and Sons,
    New York, 1960.

2. Rossi, Bruno: High Energy Particles.   Prentice-Hall, Inc.,
    Englewood Cliffs, N.J., 1961.

3. Bethe, H. A., and Heitler, W.:   Proceedings of the Royal Society
    (London), A146, 83, 1934.

4. Compton, Arthur H., and Allison, Samuel K.:   X-Rays in Theory and
    Experiment.   D. Van Nostrand Company, Inc., New York, 1935.

5. Webster, D. L.:   Physical Review.   13, 303, 1919.

6. Nicholas, W. W.:   Bureau of Standards Journal of Research.   2, 827,
    1929.

7. Koch, H. W., and Motz, J. W.:   Reviews of Modern Physics.   31,
    No. 4, 920, Oct. 1959.

8. Evans, R. D.:   The Atomic Nucleus.   McGraw-Hill Book Company, Inc.,
    New York, 1955.

9. Wright, Kenneth A., and Trump, John G.:   Journal of Applied Physics.
    33, No. 2, 687, Feb. 1962.

10. Goudsmit, S., and Saunderson, J. L.:   Physical Review.   57, 24, 1939.

11. Berger, Martin J.:   Monte Carlo Calculation of the Penetration and
    Diffusion of Fast Charged Particles.   Chapter V of Methods in
    Computational Physics, 1.   Edited by Berni Alder, Sidney Fernback,
    and Manuel Rotenberg.   Academic Press, New York, 1963.

12. Grodstein, Gladys White: National Bureau of Standards Circular

No. 583, April 30, 1957.

VITA

David Neil Ferguson

Born in Gastonia, North Carolina, December 29, 1934. Graduated from Ashley High School in that city, June, 1953; Bachelor of Science in Nuclear Engineering, North Carolina State University, May 1959.

In September 1961, the author enrolled at the College of William and Mary as a graduate student in Physics.
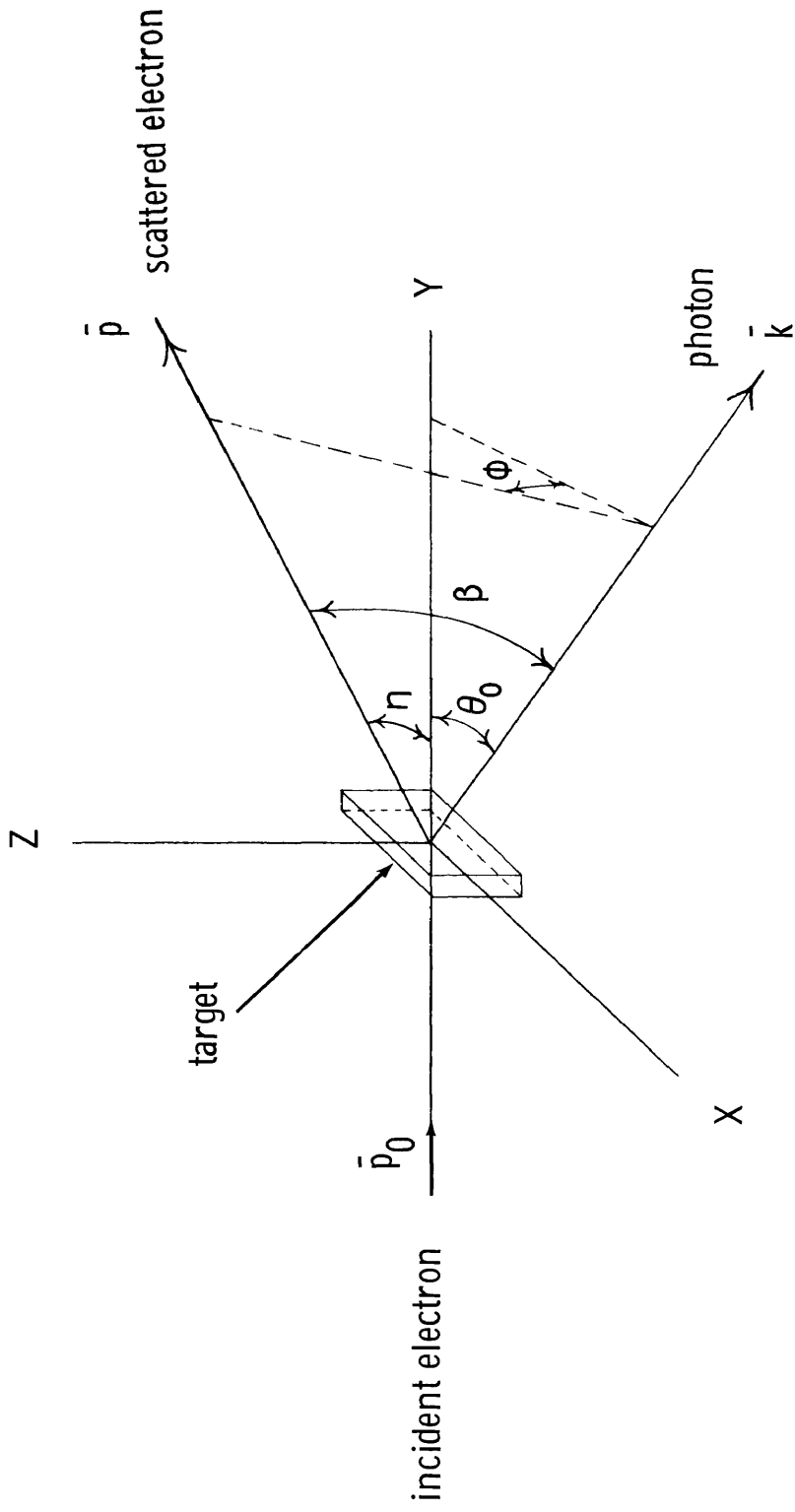
Figure 1.- Geometry for bremsstrahlung emission.
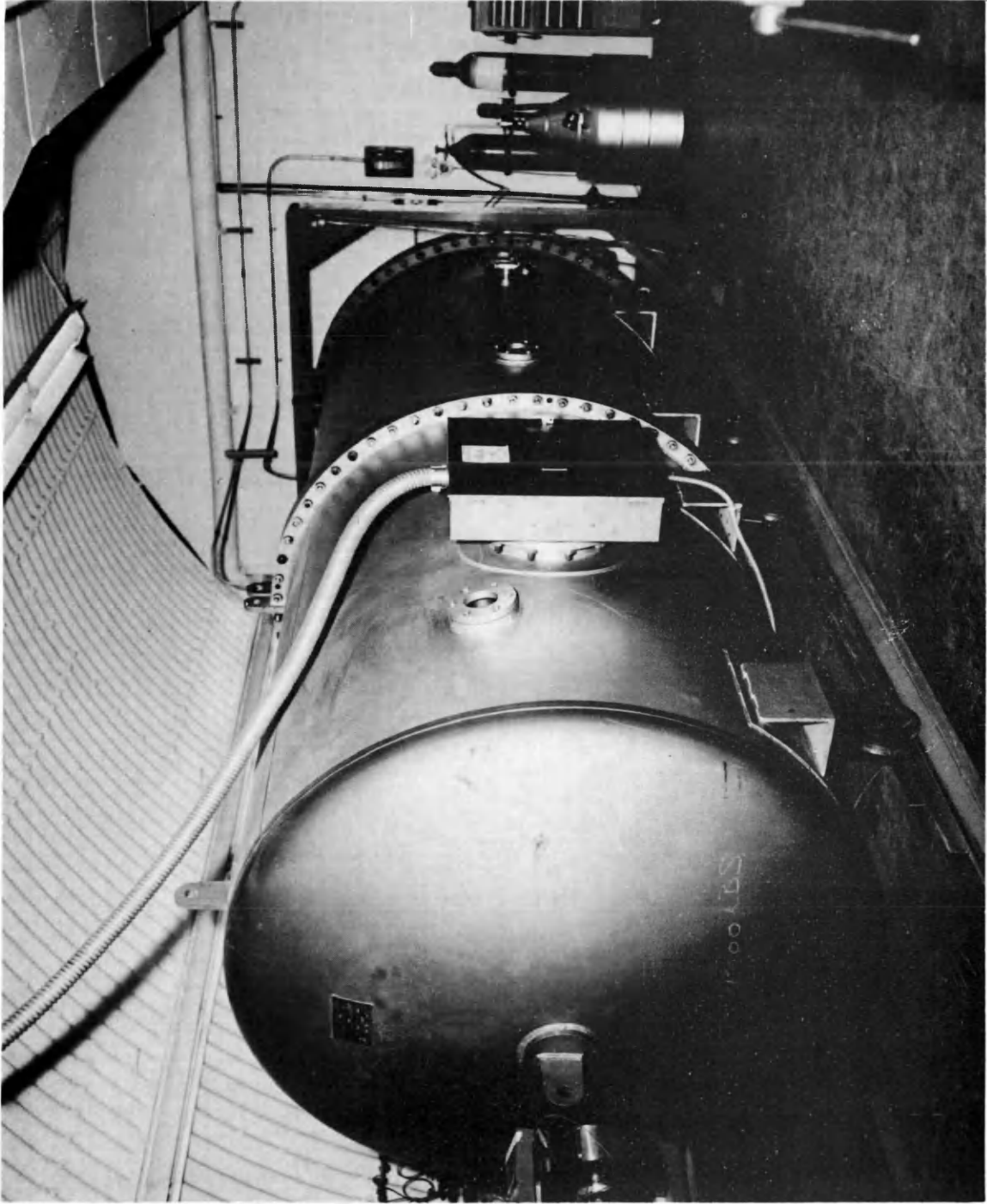
Figure 2.- Pressure vessel enclosure for Dynamitron accelerator apparatus.

1 Target chamber

2 Distribution table

3 Beam tube

4 Vacuum pump

5 Vacuum cross

6 Gate valve

7 Extension tube

8 Beam focusing magnets

9 To Dynamitron Accelerator
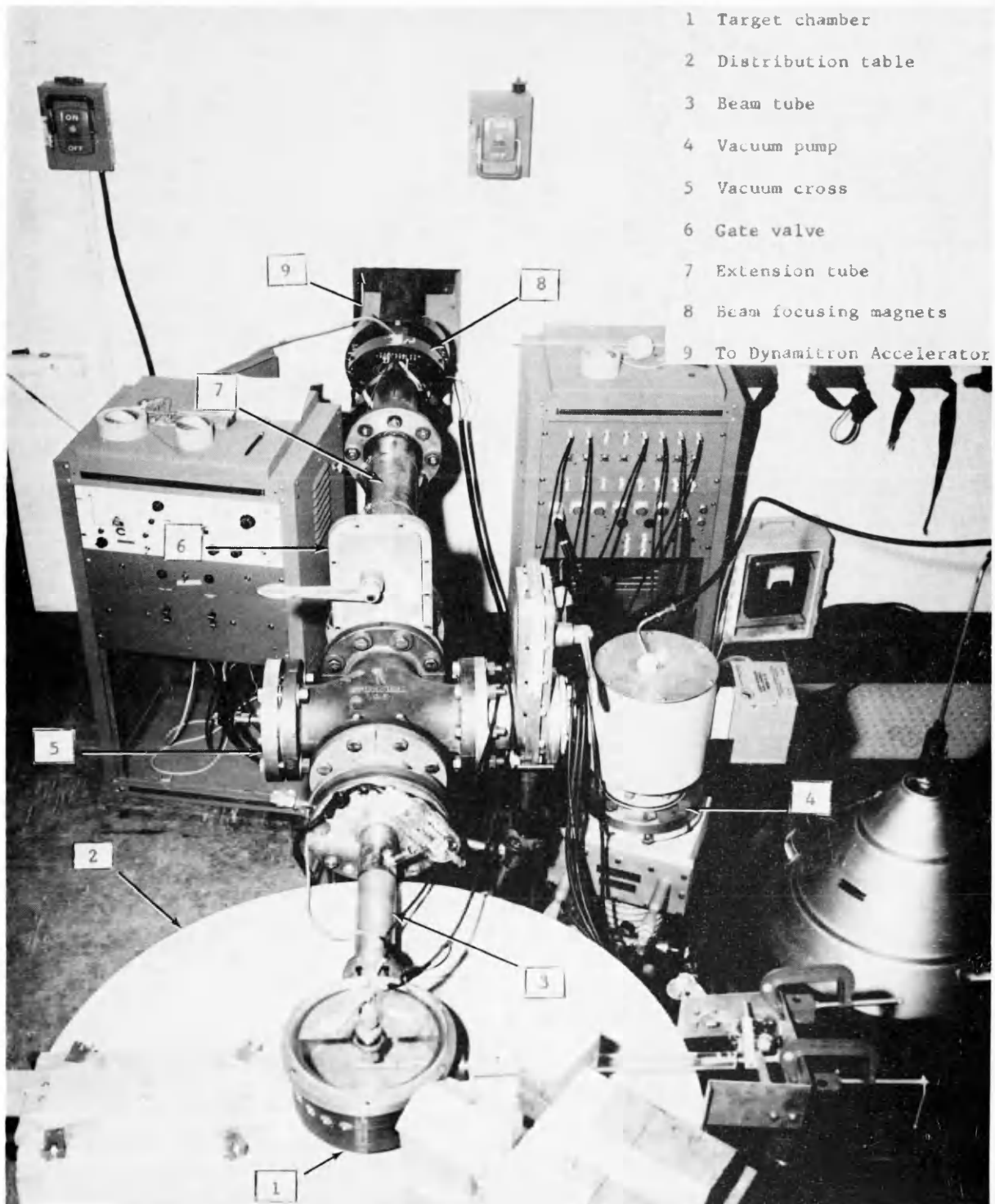
Figure 3.- Experimental assembly for bremsstrahlung measurement.

1 Lead enclosure for moveable detector
2 Target chamber
3 Stationary detector
4 Beam tube
5 Distribution table
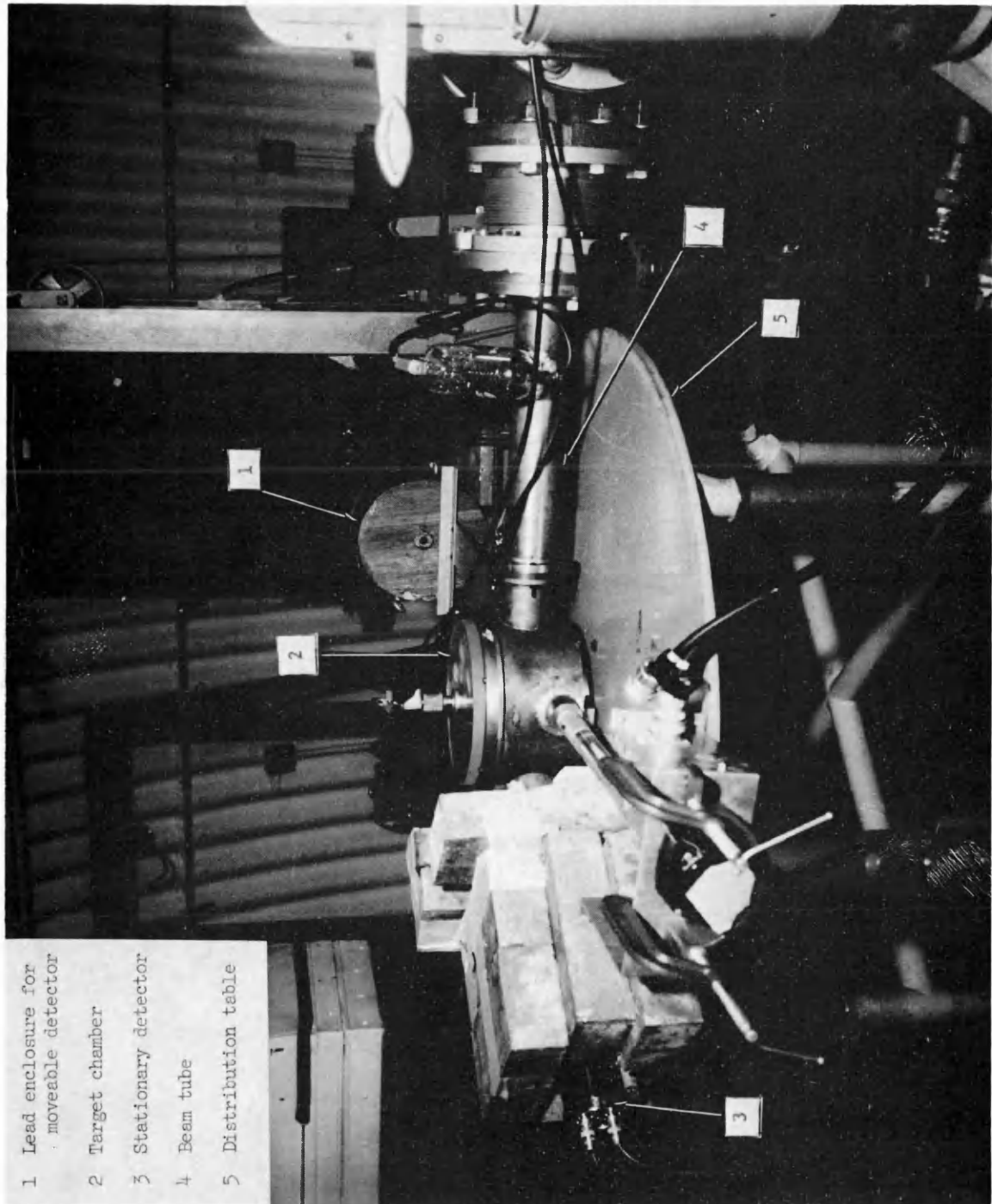
Figure 4.- Mounting arrangement for target chamber.

Stationary detector

Distribution table

Bellows

60°

16"

Beam tube

4"

Target chamber

36"

Rotating arm

Lead collimator

6"

Moveable detector

14"

Support for
collimator

9"
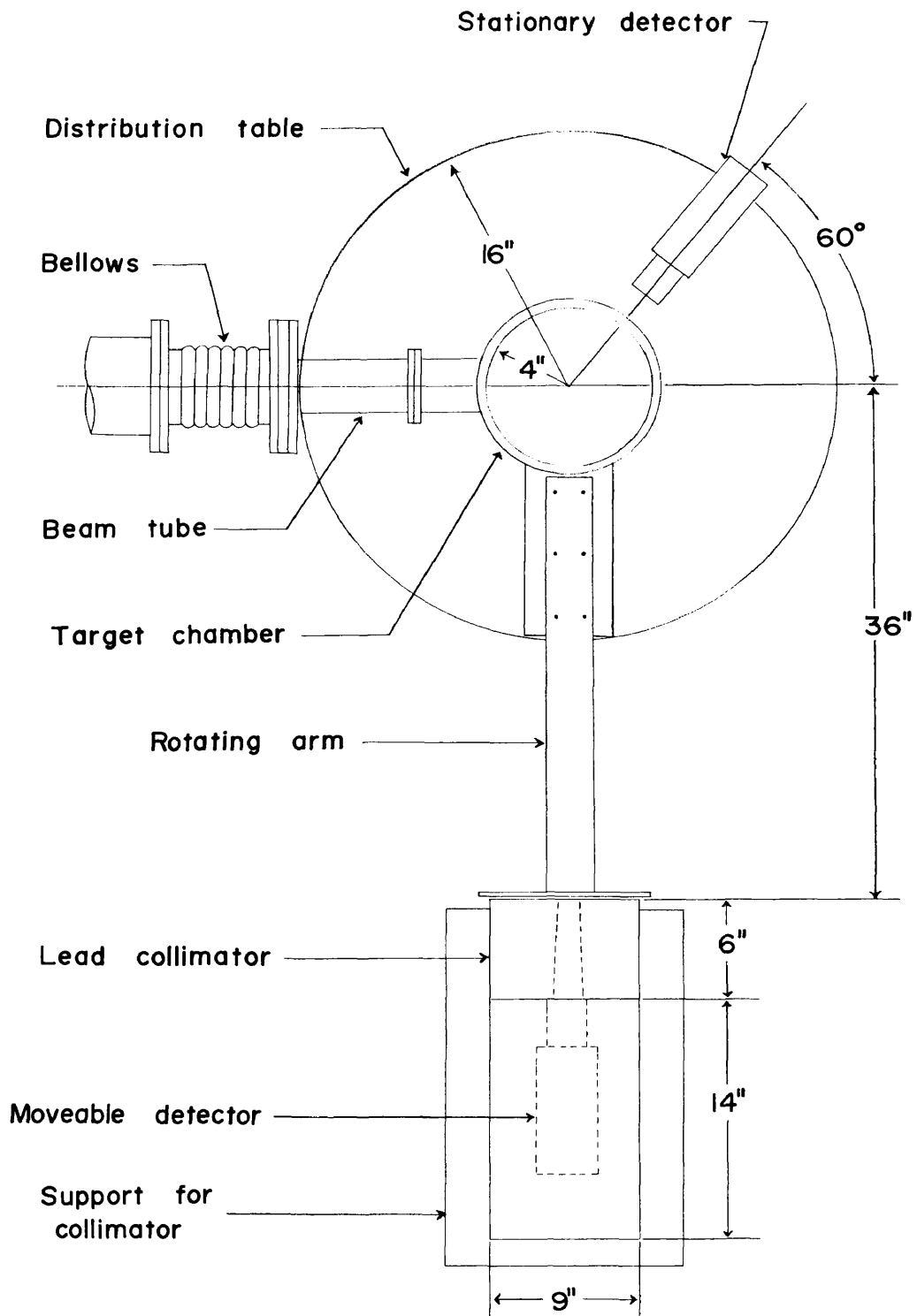
Figure 5.- Schematic of the detector arrangement.
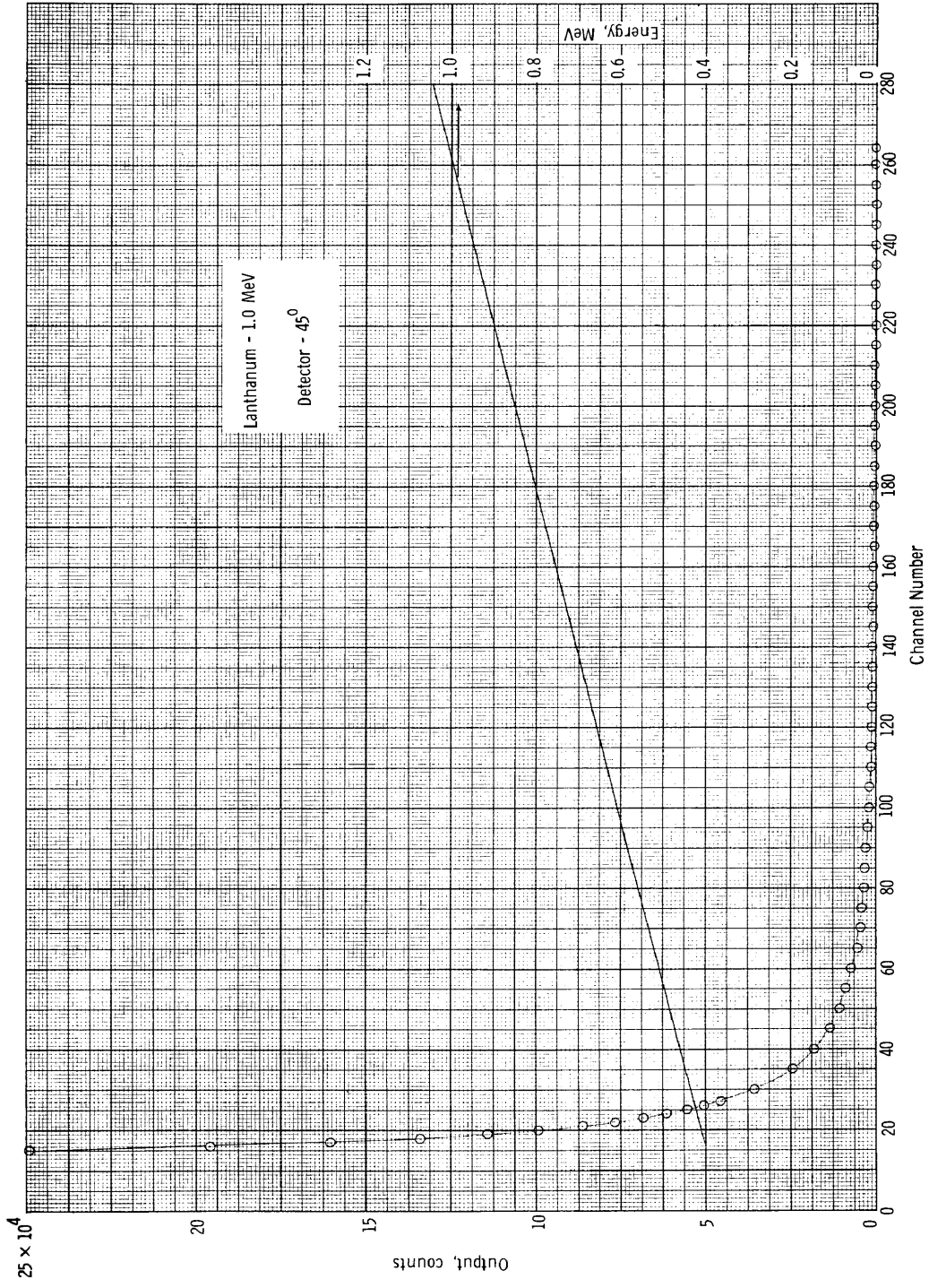
Figure 6.- Spectrum for bremsstrahlung photons in the range 0.4 MeV to 1.0 MeV observed at a detector angle of 45° with respect to a beam of 1.0 MeV electrons incident on lanthanum. No corrections have been made to the spectrum.
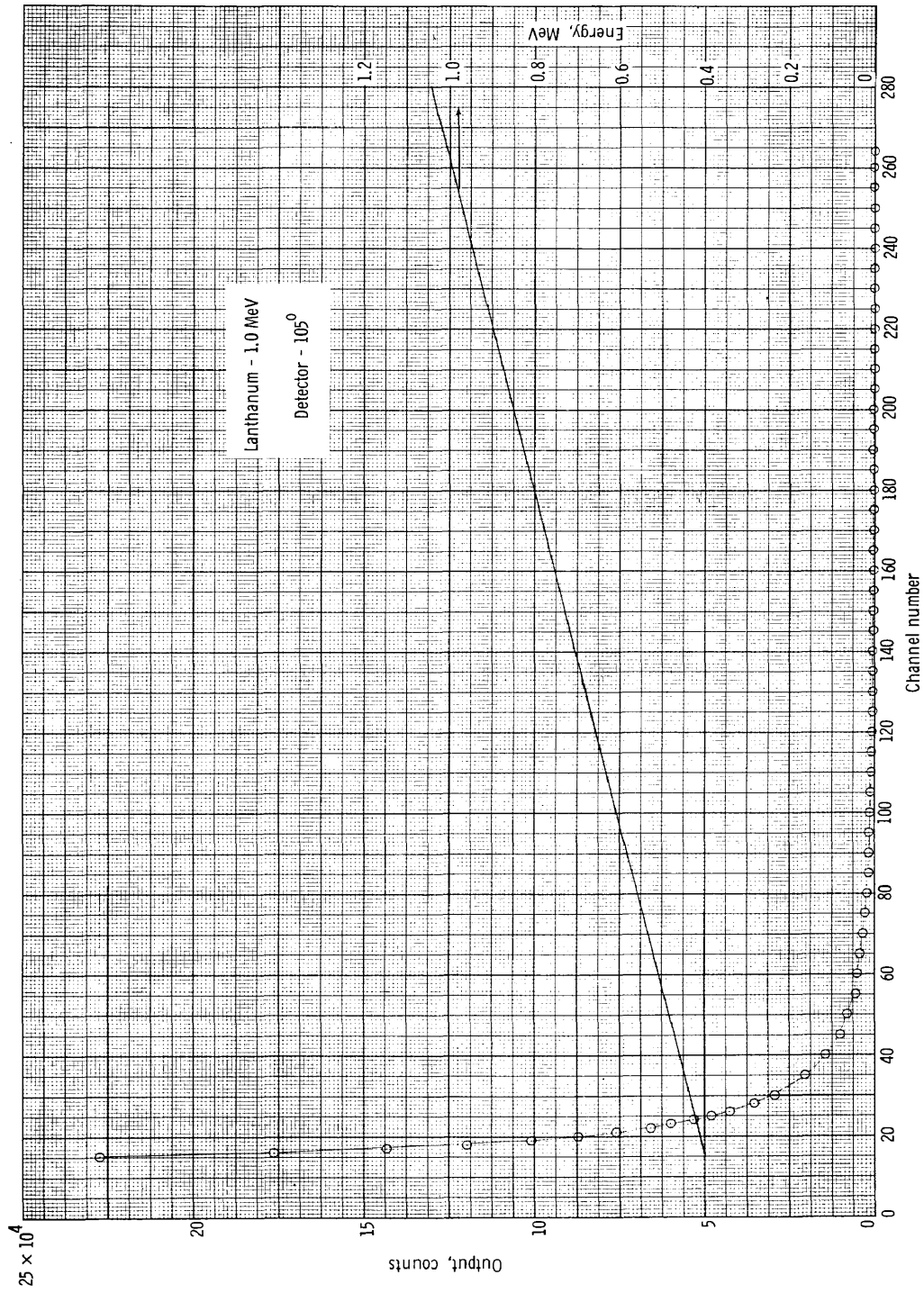
Figure 7.- Spectrum for bremsstrahlung photons in the range 0.4 MeV to 1.0 MeV observed at a detector angle of 105° with respect to a beam of 1.0 MeV electrons incident on lanthanum. No corrections have been made to the spectrum.
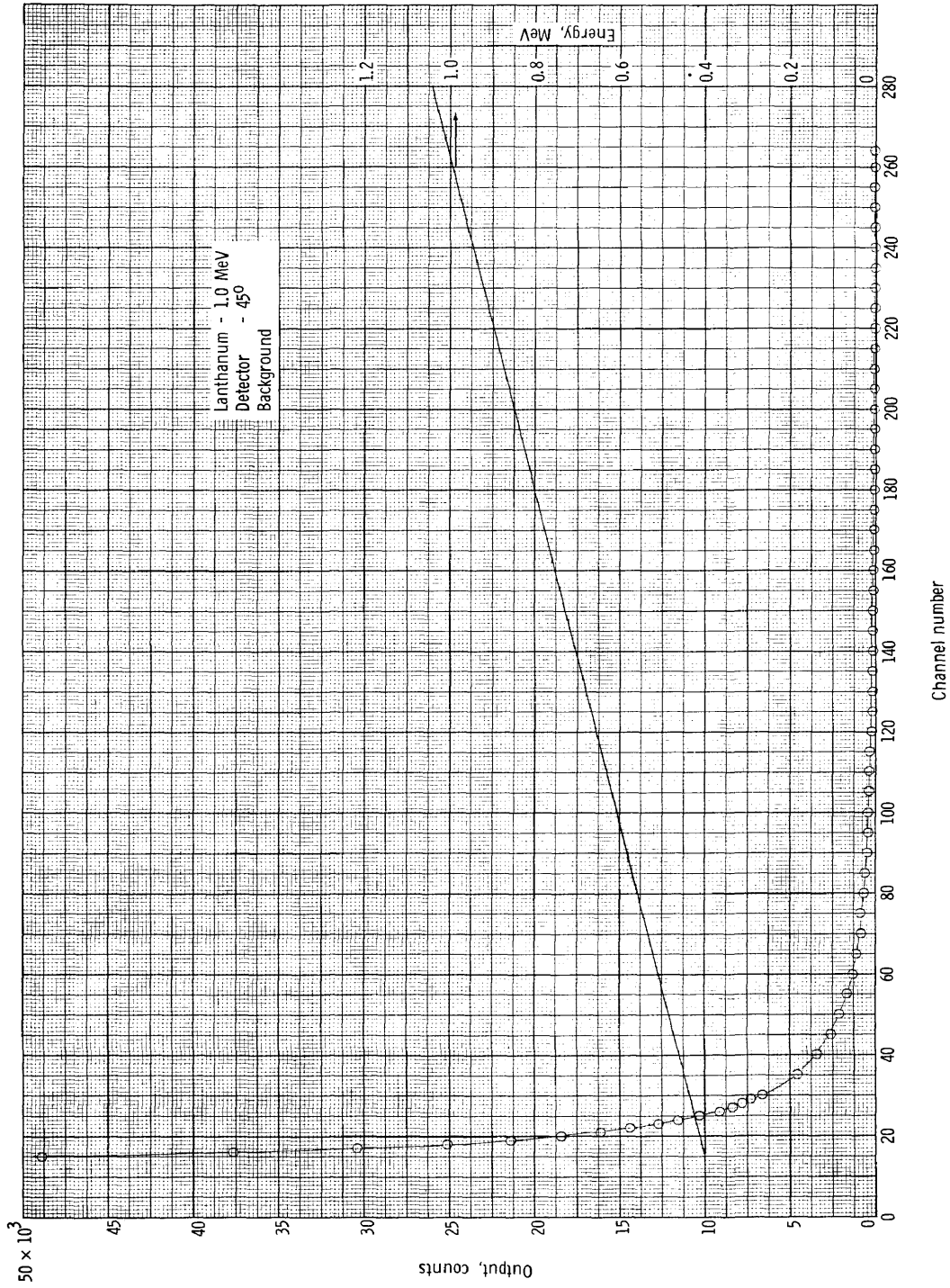
Figure 8.- Spectrum for bremsstrahlung photons in the range 0.4 MeV to 1.0 MeV observed when the target was removed and 1.0 MeV electrons struck the back of the target chamber. The detector was at an angle of 45° relative to the beam direction. No corrections have been made to the spectrum.
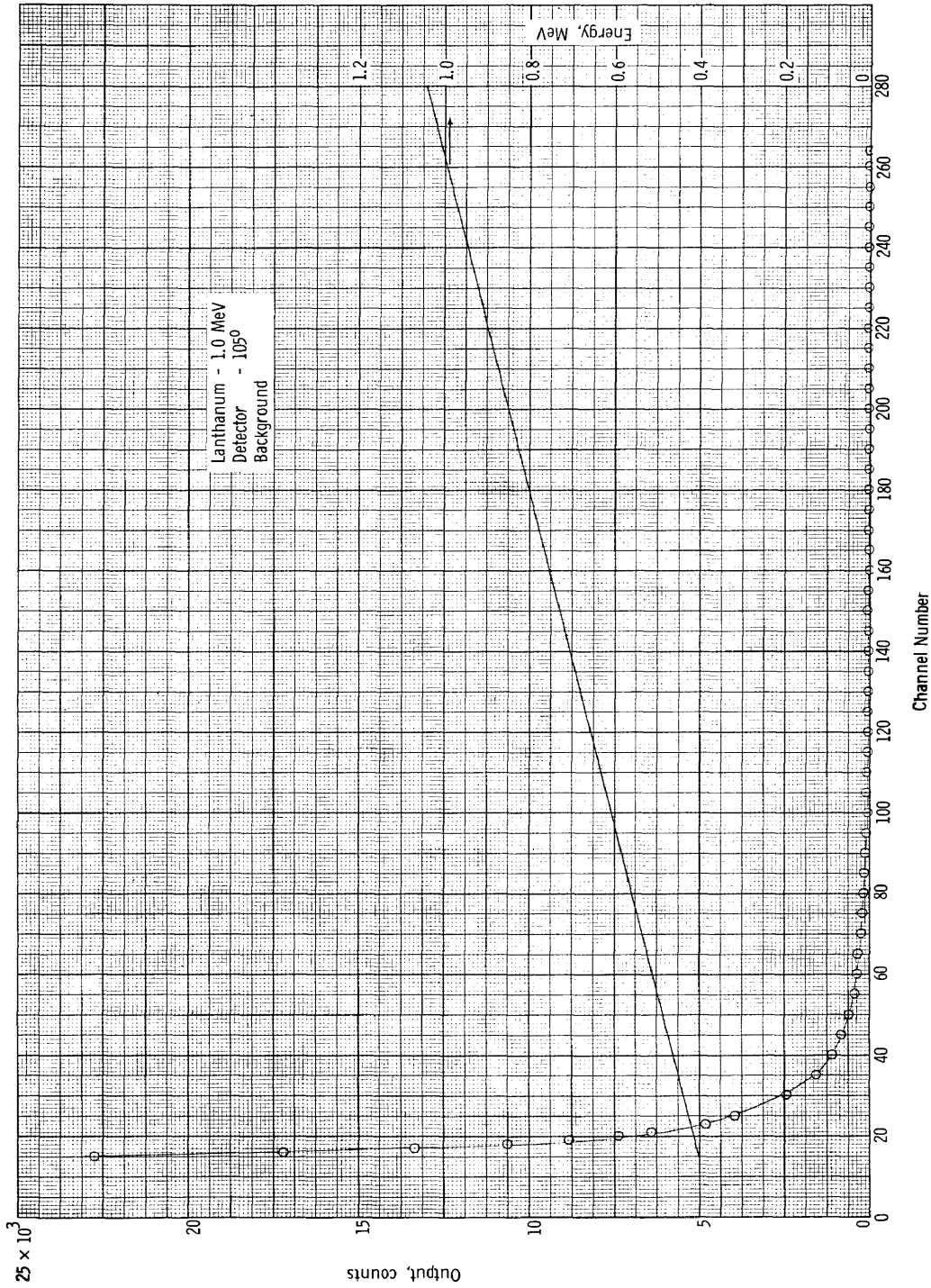
Figure 9.- Spectrum for bremsstrahlung photons in the range 0.4 MeV to 1.0 MeV observed when the target was removed and 1.0 MeV electrons struck the back of the target chamber. The detector was at an angle of 105° relative to the beam direction. No corrections have been made to the spectrum.
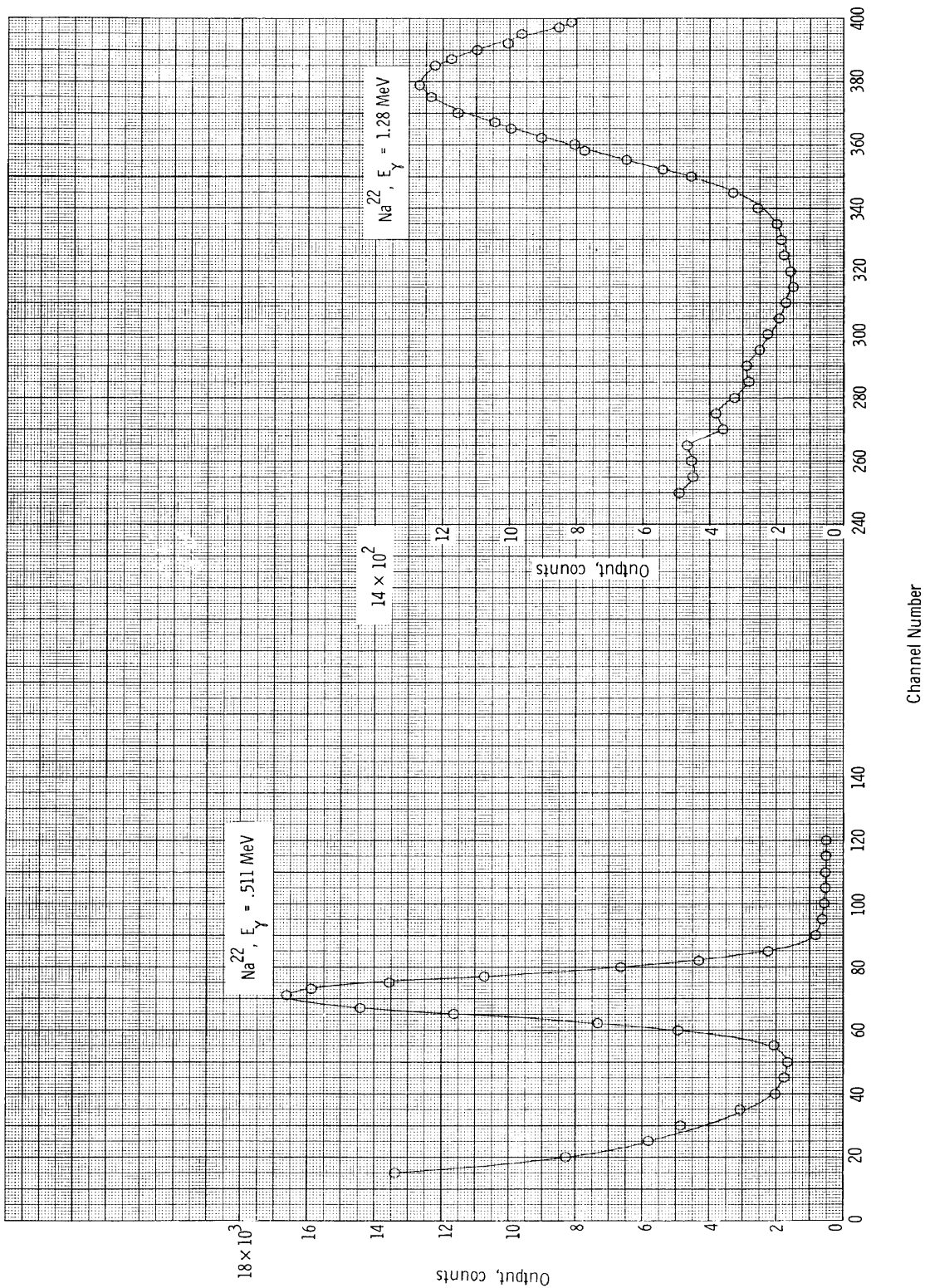
Figure 10.- Response of the detector to gamma rays from Na^{22}.
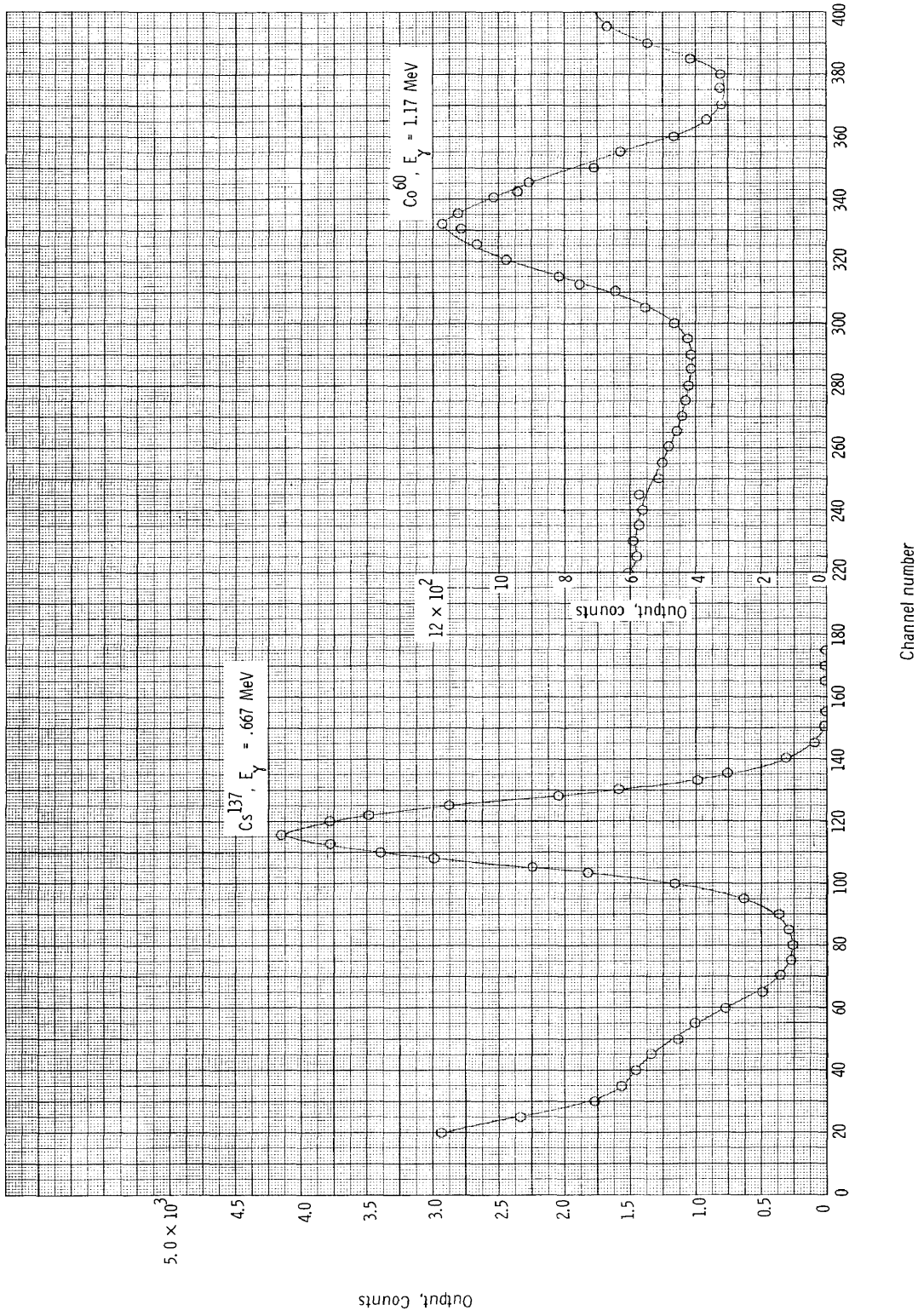
Figure 11.- Response of the detector to gamma rays from Cs^{137} and Co^{60}.
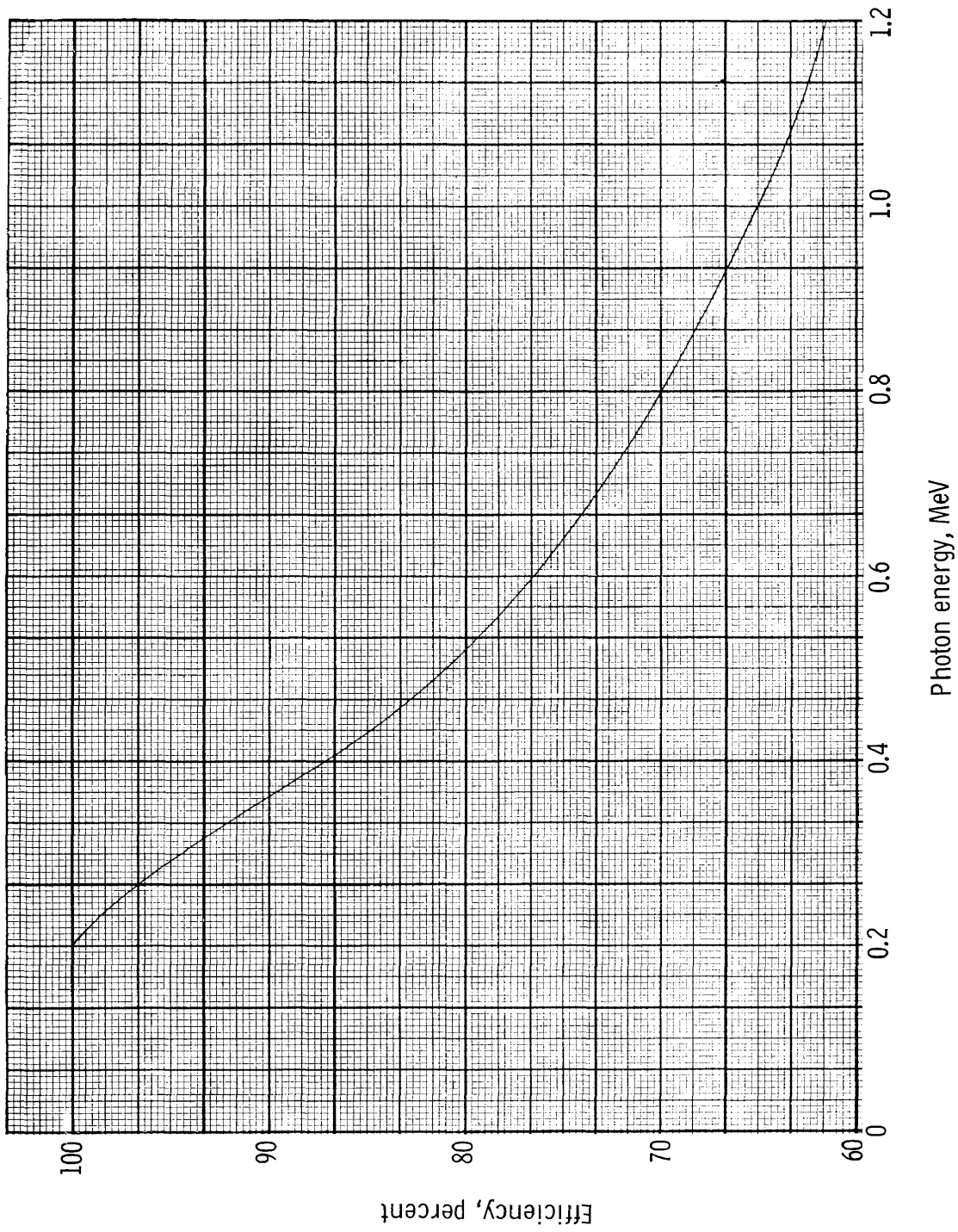
Figure 12.- Efficiency of the 2-inch by 2-inch cylindrical sodium iodide crystal. The absorption coefficients in the sodium iodide have been taken from NBS circular No. 583.
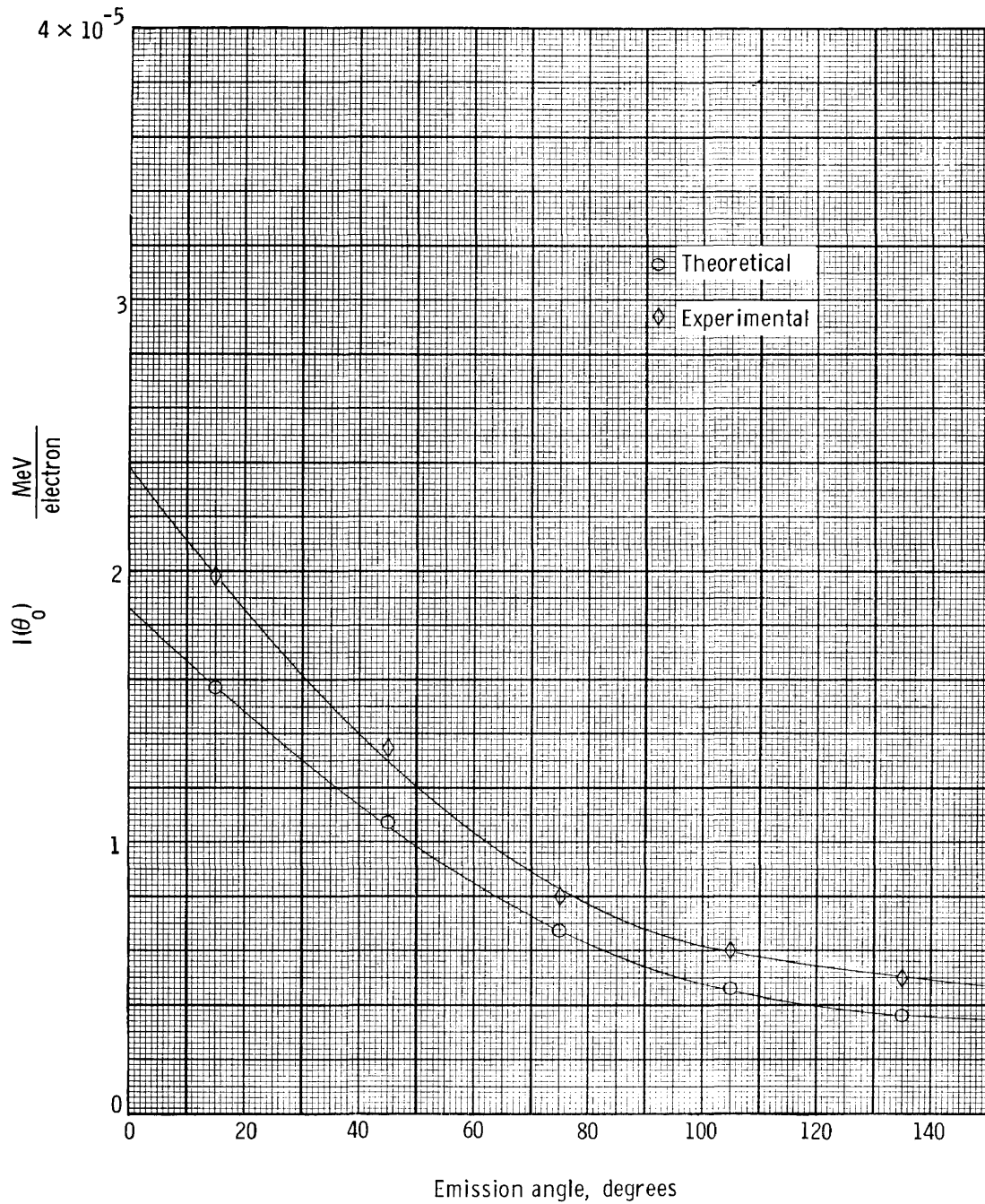
Figure 13.- Comparison of theoretical and experimental angular
distribution of 0.4 to 1.0 MeV bremsstrahlung emitted when
1.0 MeV electrons bombard thick lanthanum targets. The
encircled points are the Born-approximation theoretical
bremsstrahlung intensities.
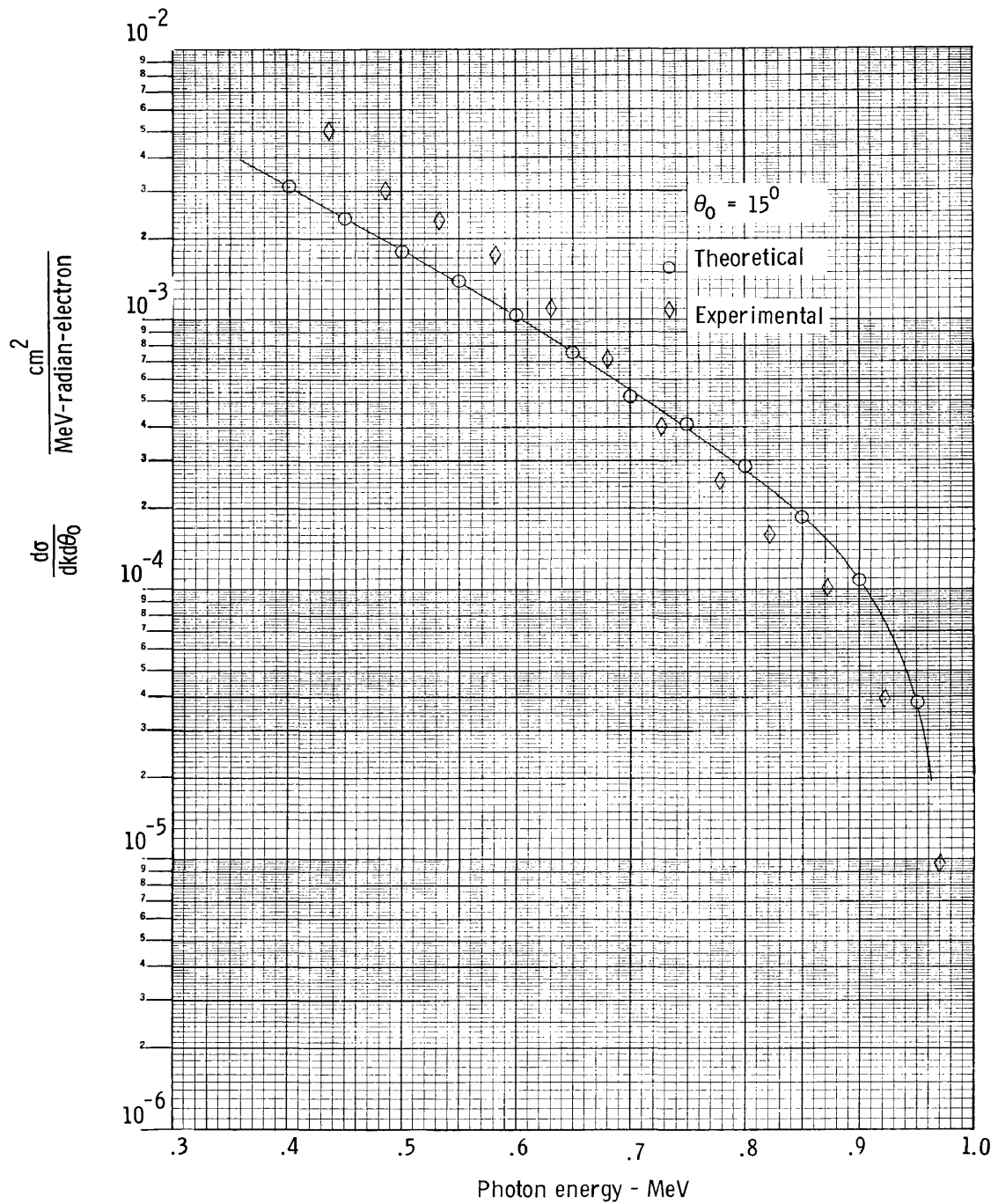
Figure 14.- Bremsstrahlung cross-section differential with respect to
photon energy and emission angle for 1.0 MeV electrons on lanthanum.
The encircled points are the Born-approximation theoretical cross
section. The photon emission angle is 15°.
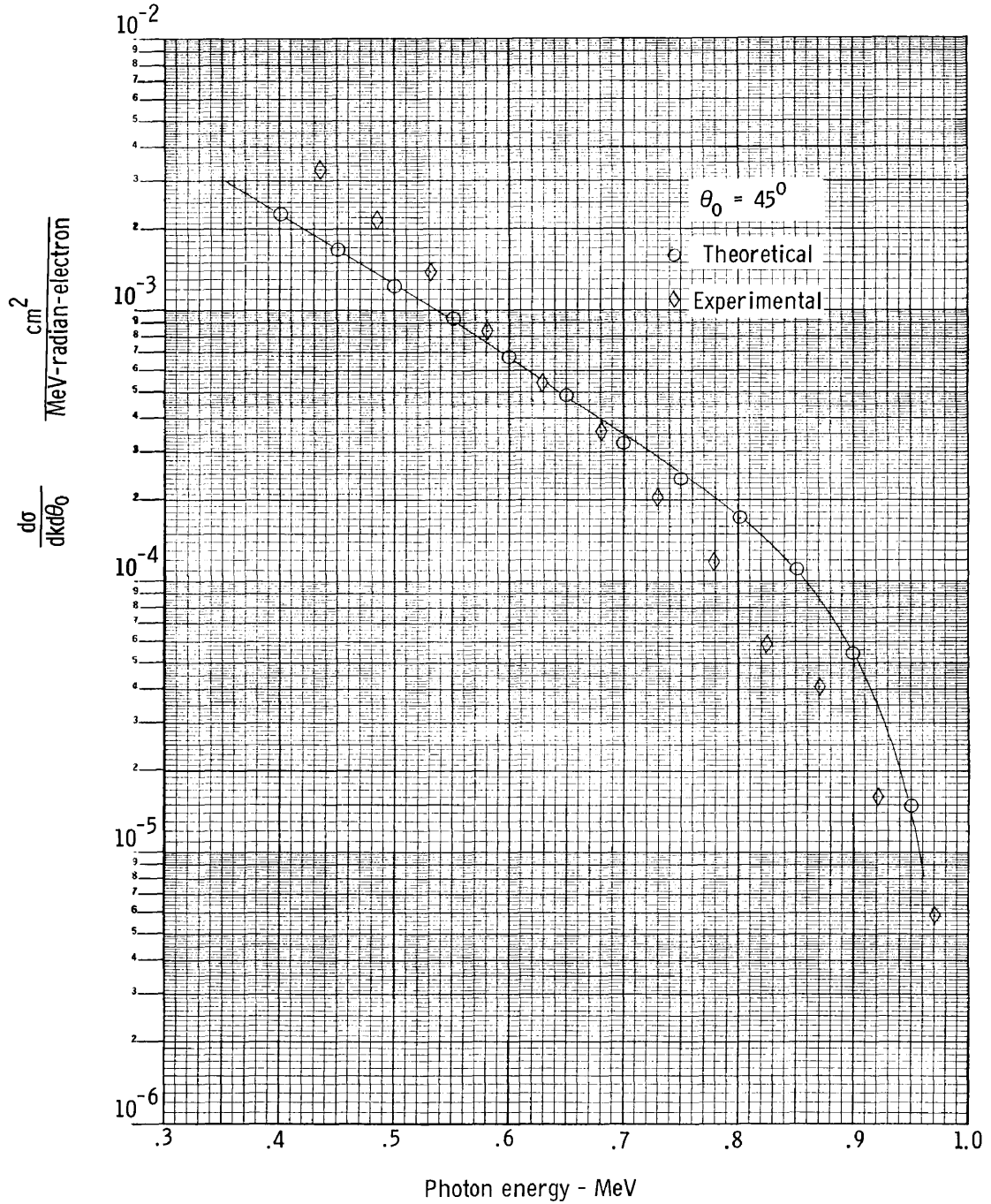
Figure 15.- Bremsstrahlung cross-section differential with respect to
photon energy and emission angle for 1.0 MeV electrons on lanthanum.
The encircled points are the Born-approximation theoretical cross
section. The photon emission angle is 45°.
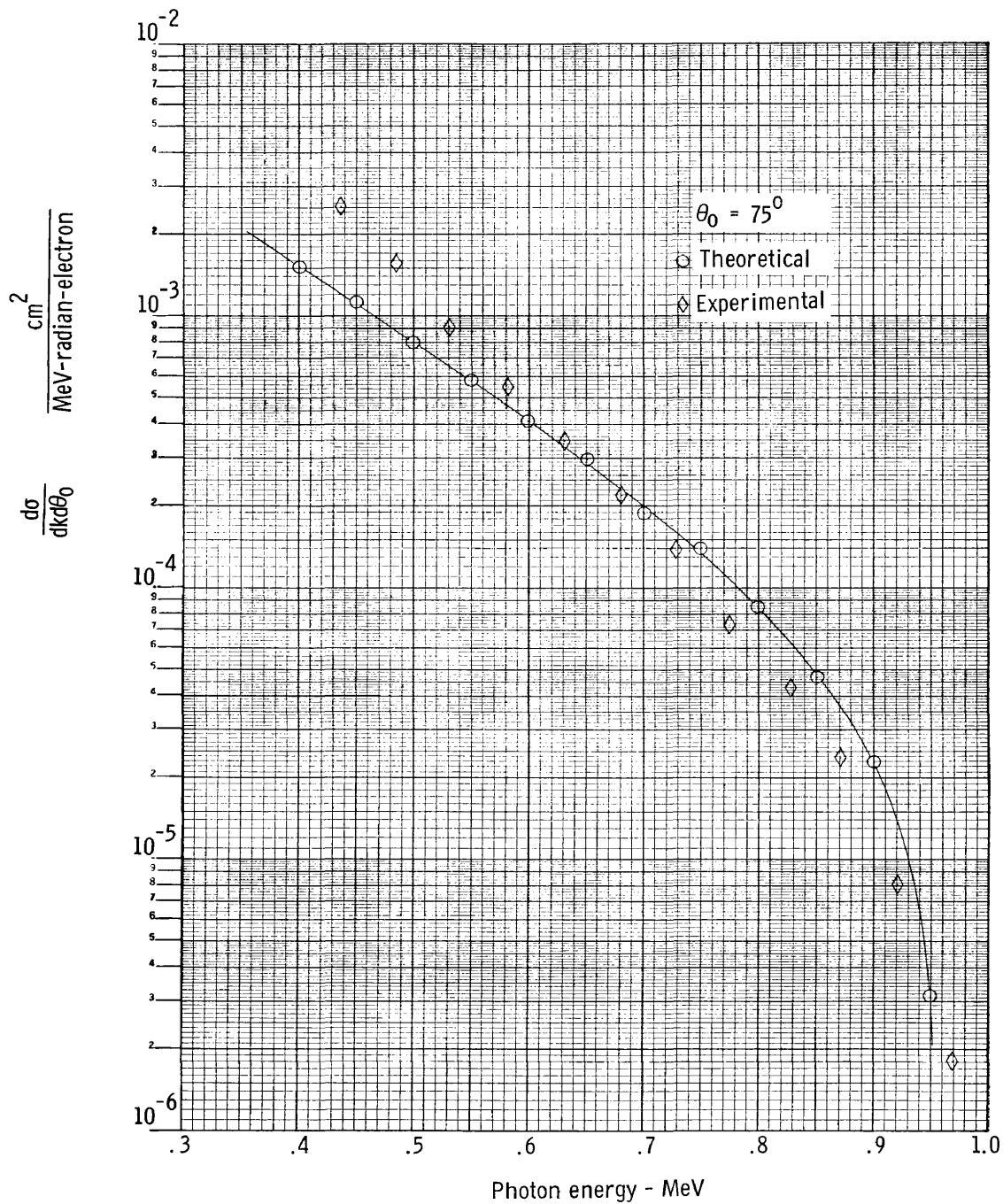
Figure 16.- Bremsstrahlung cross-section differential with respect to photon energy and emission angle for 1.0 MeV electrons on lanthanum. The encircled points are the Born-approximation theoretical cross section. The photon emission angle is 75°.
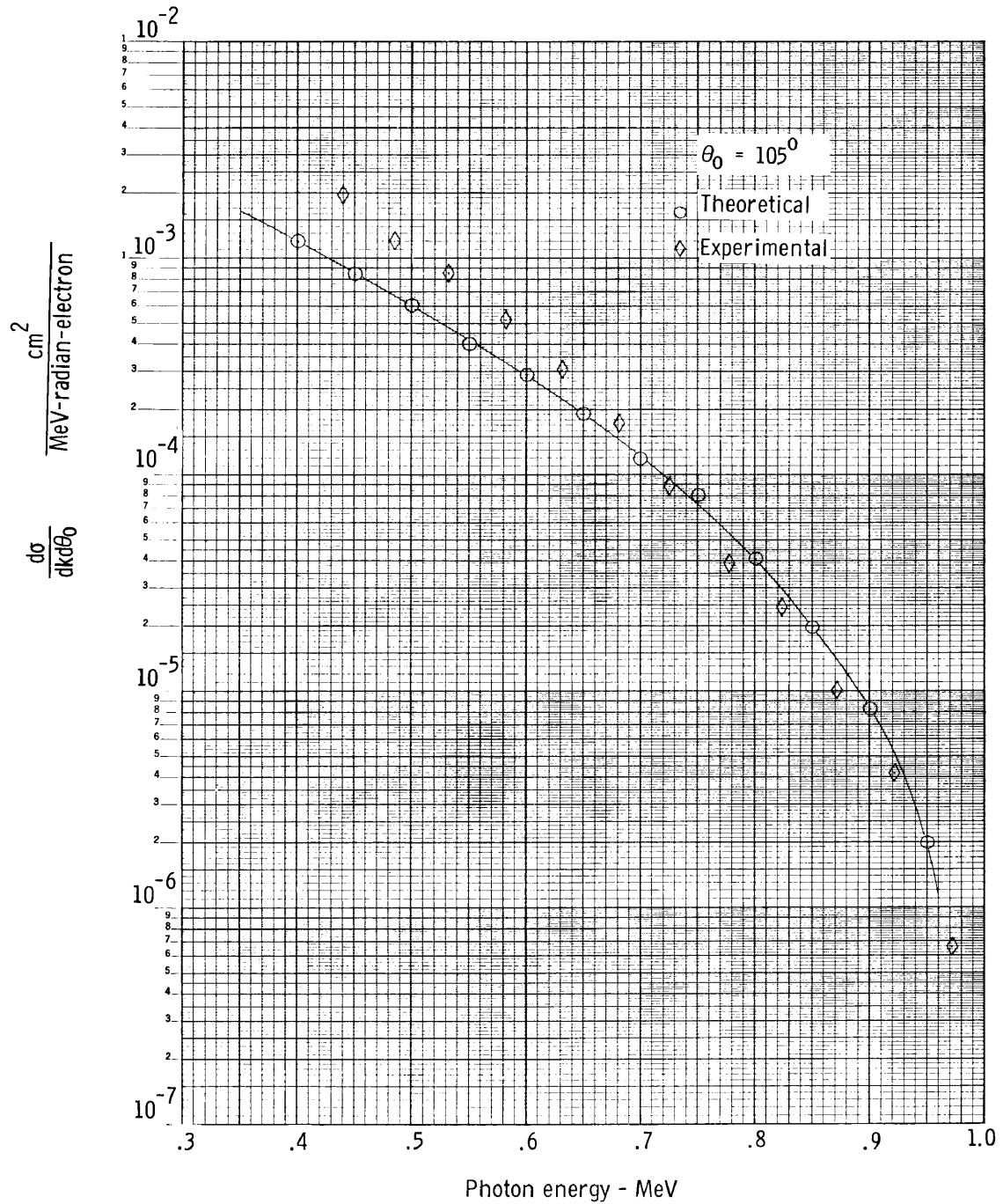
Figure 17.- Bremsstrahlung cross-section differential with respect to photon energy and emission angle for 1.0 MeV electrons on lanthanum. The encircled points are the Born-approximation theoretical cross section. The photon emission angle is 105°.
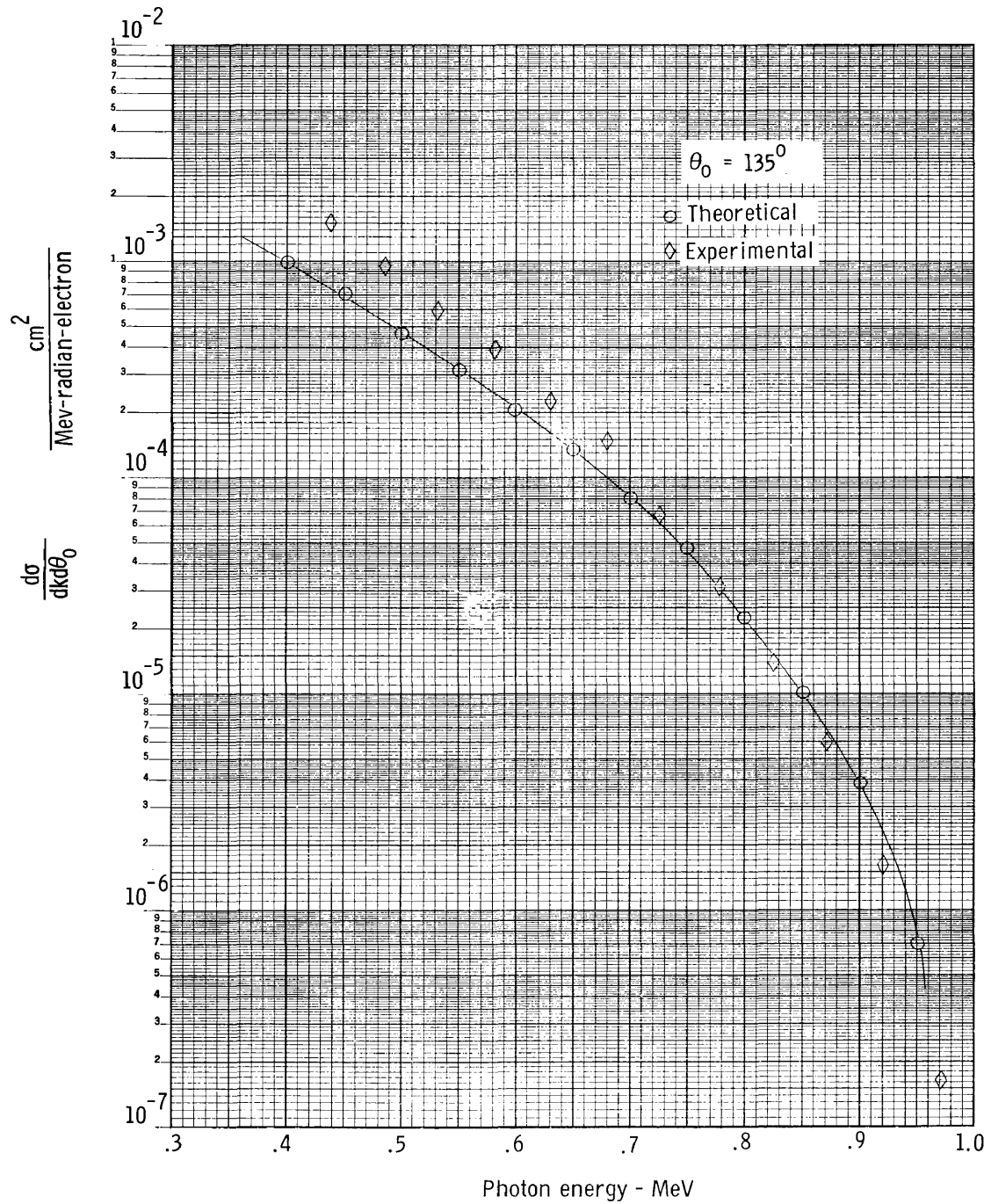
Figure 18.- Bremsstrahlung cross-section differential with respect to photon energy and emission angle for 1.0 MeV electrons on lanthanum. The encircled points are the Born-approximation theoretical cross section. The photon emission angle is 135°.
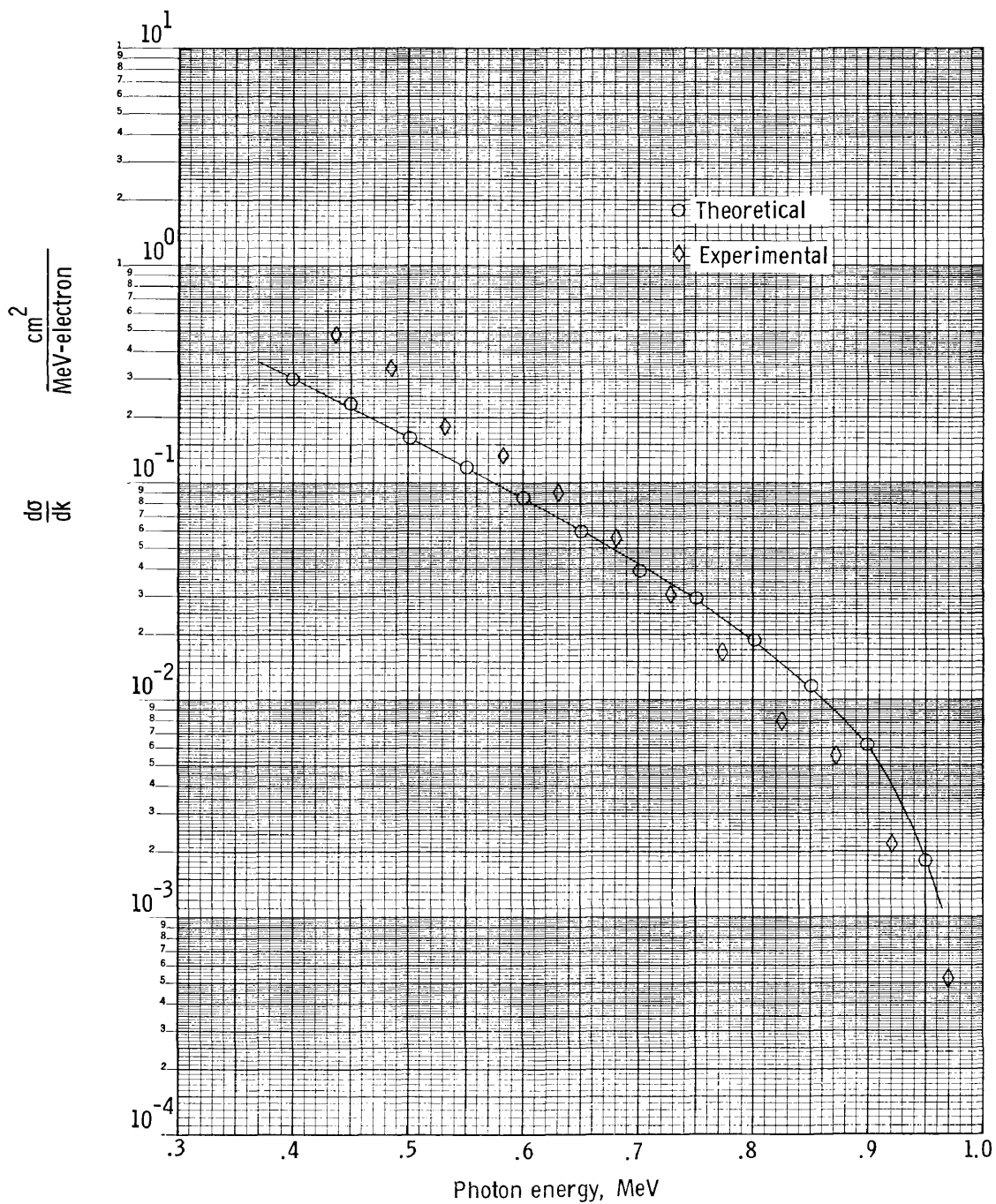
Figure 19.- Dependence of the bremsstrahlung cross section integrated
over photon emission angle on the photon energy for 1.0 MeV electrons
incident on a lanthanum thick target. The encircled points are the
Born-approximation theoretical cross sections.